

Distribution characteristics of summer precipitation raindrop spectrum in Qinghai–Tibet Plateau

Fuzeng Wang^{1,2}, Yuanyu Duan¹, Yao Huo¹, Yaxi Cao¹, Qiusong Wang¹, Tong Zhang²,
Junqing Liu³, Guangmin Cao⁴

¹College of Electronic Engineering, Chengdu University of Information Technology, Chengdu 610225,
China

²Key Laboratory of Land Surface Process and Climate Change in Cold and Arid Regions, Chinese
Academy of Sciences, Lanzhou 730000, China

³Weather Modification Center for Tibet, Lhasa 850000, China

⁴Heilongjiang Meteorological Data center, Harbin 150000, China

Correspondence to: Guangmin Cao(ccgm909@163.com)

Abstract: To enhance the precision of precipitation forecasting in the Qinghai–Tibet Plateau region, a comprehensive study of both macro– and micro–characteristics of local precipitation is imperative. In this study, we investigated the particle size distribution, droplet velocity, droplet number density, Z (Radar reflectivity) – I (Rainfall intensity) relationship, and Gamma distribution of precipitation droplet spectra with a single precipitation duration of at least 20 minutes and precipitation of 5 mm or more at four stations (Nyalam, Lhasa, Shigatse, and Naqu) in Tibet during the recent years from June to August. The results are as follows: (1) In the fitting relationship curve between precipitation raindrop spectral particle size and falling speed at the four stations in Tibet, when the particle size was less than 1.5 mm, the four lines essentially coincided. When the particle size exceeded 1.5 mm, the speed in Nyalam was the highest, followed by Naqu, and the speed in Lhasa was the lowest. The falling speed of particles correlated with altitude. (2) The six microphysical characteristics(mean diameter (D_m), average volume diameter (D_v), mode diameter (D_d), dominant diameter (D_p), and median diameter (D_{nd})) at the four stations have different correlation relationships with altitude under different rainfall intensities. D_m exhibits a negative correlation with altitude at the same rainfall intensity; in contrast, D_v shows a positive correlation with altitude. For microphysical parameters such as D_d and D_p , a rainfall intensity of $10\text{mm}\cdot\text{h}^{-1}$ serves as the boundary line, and they have different correlation relationships with altitude under the same rainfall intensity level. (3) The Z – I relationships at the four stations exhibited variations. Owing to the proximity in altitude between Lhasa and Shigatse, as well as

30 between Nyalam and Nagqu, the coefficients a and index b in the $Z-I$ relationships of the two groups
31 of sites were relatively similar. (4) The fitting curves of the Exponential and Gamma distributions of
32 the precipitation particle size at the aforementioned four stations are largely comparable. The
33 Exponential distribution fitting exhibits a slightly better effect. The parameter μ in Gamma distribution
34 decreases with the increase of altitude, while N_0 and λ in Exponential distribution show a clear upward
35 trend with altitude.

36 **1. Introduction**

37 The microphysical processes of cloud and precipitation over the Qinghai–Tibet Plateau significantly
38 differ from those in low–altitude regions due to the high average altitude and complex, changeable
39 terrain, resulting in a strong ground heating effect. Due to the terrain's influence, the plateau area has a
40 limited number of observation stations, leading to a scarcity of precipitation records. Based on three
41 atmospheric scientific experiments conducted over the Qinghai–Tibet Plateau, convective clouds
42 exhibit high activity, although the precipitation intensity is moderate(Li et al., 2014; Jiang et al., 2002;
43 Xu et al., 2006; Li et al., 2001). In the central part of the Plateau, convective clouds constitute 4% to
44 21%, with cumulonimbus clouds representing 21%. Additionally, the frequency of severe weather, such
45 as thunderstorms and hail, surpasses that in other regions. In the majority of Qinghai–Tibet Plateau
46 areas, convective cloud precipitation constitutes over 90% of the total (Chang and Guo, 2016).
47 Particularly during the rainy season, convective processes are frequent with smaller horizontal scales,
48 weaker intensities, and shorter durations. Due to observational constraints, short–term tests and satellite
49 data (e.g., TRMM, CloudSat, and Aqua) are employed to investigate Tibetan Plateau precipitation, with
50 a focus on liquid precipitation characteristics, including seasonal and diurnal variations and convective
51 activity's liquid drop spectrum inversion(Ruan et al., 2015; Liu et al., 2015; Xiong et al., 2019; Zhang
52 et al., 2018). The scarcity of observational data on cloud precipitation's physical processes in the
53 Qinghai–Tibet Plateau results in limited studies on microscopic parameters' characteristics. The recent
54 installation of a laser raindrop spectrometer enables a comprehensive understanding of the plateau's
55 precipitation microphysical parameters through the study of raindrop spectral parameters and
56 distribution characteristics in various regions.

57 Some studies have explored the spectral characteristics of raindrops over the Tibetan Plateau. Yu Jianyu

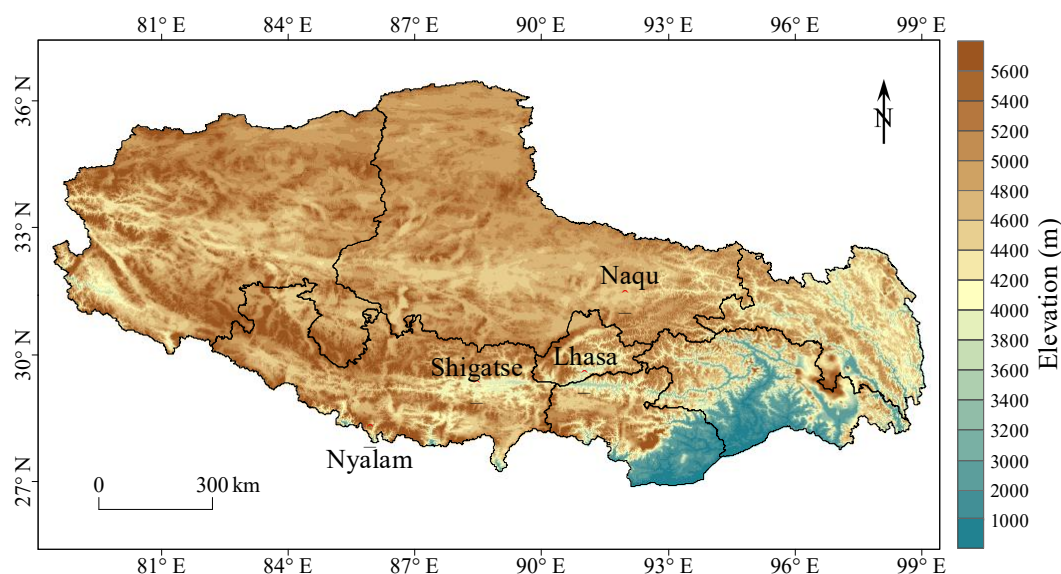
58 et al. and Shu Lei et al. conducted analyses on the raindrop spectrum characteristics of various clouds
59 in the Naqu and Yushu regions of the Qinghai–Tibet Plateau(Yu et al., 2020; Shu et al., 2021). Li
60 Shanshan et al. investigated raindrop spectral characteristics at different elevations on the eastern slope
61 of the Qinghai–Tibet Plateau. They discovered that the average spectrum of raindrop number
62 concentration at various elevations conforms to the Gamma function distribution. Moreover, light
63 precipitation and heavy precipitation exhibit distinct raindrop spectral characteristics(Li et al., 2020).
64 The aforementioned research was conducted in Naqu and Yushu areas in the Qinghai–Tibet Plateau, as
65 well as the west Sichuan Plateau area. However, there is a limited number of studies on the spectral
66 characteristics and distribution rules of cloud precipitation raindrops in various regions of the Tibetan
67 Plateau. The analysis of raindrop spectrum characteristics in the Naqu region, as mentioned earlier, was
68 conducted only during the summer months from June to August 2014. In this study, we used raindrop
69 spectrum data from the Naqu region spanning 2017 to 2020, building upon and extending previous
70 research. We analyzed the temporal variation of the raindrop spectrum in convective cloud precipitation
71 across various regions and examined differences in raindrop spectra among these regions. We
72 conducted a systematic analysis of raindrop spectrum data associated with moderate rain from four
73 stations with varying altitudes, longitudes, and latitudes. We compared and analyzed the differences in
74 drop spectrum characteristics among these four stations, which is of great significance for enhancing
75 the scientific understanding of precipitation's influence in the plateau region.
76 The objective of this study is to enhance the understanding of raindrop spectrum characteristics at
77 various elevations of the Tibetan Plateau. The findings of this study will establish a foundation for
78 comprehending precipitation characteristics and improving precipitation forecasts at diverse elevations
79 of the Tibetan Plateau. This study is structured as follows: Data sources and research methods are
80 described in Section 2. The analysis results are presented in Section 3 while the conclusion and
81 discussion are provided in Section 4.

82 **2. Data and methods**

83 **2.1. Data collection**

84 The data obtained for this study consist of raindrop spectrum data from four meteorological stations
85 (i.e., Nyalam, Lhasa, Shigatse, and Naqu) in Tibet. Owing to its unique climate environment, snowfall

86 occurs time to time from September to May. Data from June to August is selected to analyze the
 87 precipitation raindrop spectrum process in this study. The precipitation data selection criteria include a
 88 precipitation process duration exceeding 20 minutes and a single precipitation process with rainfall
 89 greater than 5mm. As the frequency of convective clouds in most areas of the Qinghai–Tibet Plateau
 90 exceeds 90%, all collected samples are categorized as convective clouds in this paper. Table 1 displays
 91 the longitude, latitude, altitude, and sample numbers of the four stations. Figure 1 illustrates the
 92 geographical distribution of the four sites. The four stations cover a broad area of central Tibet from
 93 south to north, making the results representative.



94
 95 **Figure 1: Station distribution and the surrounding terrain**

96 **Table 1: Coordinates, elevation, sampling periods, and sample sizes of the four sites.**

Station	Longitude	Latitude	Elevation	Sampling period	Sample size
Nyalam	85.58° E	28.11° N	4519 m	2017–2019	11579
Lhasa	91.08° E	29.40° N	3653 m	2017–2018	8364
Shigatse	88.53° E	29.15° N	3910 m	2017–2018	14237
Naqu	92.04° E	31.29° N	4560 m	2017–2020	5630

97 **2.2. Quality Control and Quality Assurance (QA/QC)**

98 The Parsivel2 raindrop spectrometer features 32 particle size measurement channels and 32 particle
 99 velocity measurement channels. The particle size measurement range is 0.062–24.5 mm, and the
 100 particle velocity measurement range is 0.05–20.8 m s⁻¹, with a sampling time of 60 s. In comparison to
 101 the previous Parsivel raindrop spectrometer model, the Parsivel2 raindrop spectrometer utilizes infrared

102 light as its light source. This change reduces the interference of visible light, resulting in significant
 103 advancements in the measurement of raindrop size and rainfall. Following the sampling principle of the
 104 raindrop spectrometer, the instrument records the particle size and particle speed of all particles passing
 105 through the sampling surface. To mitigate the influence of sand and dust particles, it is imperative to
 106 control the quality of the fundamental data.

107 Atlas(Atlas et al., 1973) discovered a relationship between the terminal velocity of particles and the
 108 particle diameter. In an ideal windless environment, the formula for the terminal velocity of particles is:

$$\begin{cases} v=0, & x < 0.03 \\ v = 4.323 \times (x - 0.03), & 0.03 \leq x \leq 0.6 \\ v = 9.65 - 10.3 \times e^{-0.6x}, & x > 0.6 \end{cases} \quad (1)$$

109 where x represents the particle diameter in mm, and v represents the terminal velocity of the particle in
 110 m s^{-1} . Equation (1) is applicable near the ground. For other altitudes, considering the known effect of
 111 atmospheric air density on the terminal fall velocity, a correction factor for the fall velocity of raindrops,
 112 accounting for air density, as given by Atlas et al. (1973) and Foote and du Toit et al. (1969), $(\rho_0/\rho)^{0.4}$ is
 113 multiplied on the right-hand side of Equation (1). Here, ρ is the air density at the observation altitude,
 114 and ρ_0 is the air density at sea level under standard atmospheric pressure.

116 Kruger and Krajewski(Kruger and Krajewski, 2002) proposed a method to mitigate the dispersion of
 117 velocity over large samples, building on the study by Atlas. Initially, the terminal velocity was
 118 calculated based on the particle diameter and final velocity formula, and subsequently, a threshold
 119 value was set for elimination. The formula is expressed in Equation 2.

$$|v_{measured} - v_A| < 0.4v_A \quad (2)$$

120 where $v_{measured}$ represents the final velocity measured by the raindrop spectrometer, and v_A is the final
 121 velocity calculated using the final velocity formula. If the relative error falls within the specified
 122 threshold range, the data will be retained.

124 Previous studies have highlighted that the distribution of raindrop spectra exhibit distinct
 125 characteristics influenced by geographical environment and topography. Hence, utilizing the same
 126 calculation formula across different areas for raindrop spectrum elimination is likely to introduce
 127 significant errors. Therefore, we utilized historical data from a raindrop spectrum site to localize the
 128 parameters identified in the study by Atlas and incorporates them into the formula for particle
 129 elimination. Simultaneously, due to deformation occurring in raindrops during descent, the raindrop

130 spectrum data undergoes distortion and correction after quality control.

131 2.3. Raindrop spectrum parameters

132 The number density of the precipitation raindrop spectrum is defined as the total number of particles
133 per unit volume(Shi et al., 2008).

$$134 \quad N(D) = \sum_{i=1}^{32} \sum_{j=1}^{32} \frac{n_{ij}}{A \cdot \Delta T \cdot V_j} \quad (3)$$

135 where $N(D)$ is the number density parameter, in units of $\text{mm}^{-1} \text{m}^{-3}$; n_{ij} represents the number of
136 raindrops with the diameter of the i -th particle and the velocity of the j -th particle; A is the sampling
137 base area of the raindrop spectrometer (5400 mm^2); ΔT is the sampling time (60 s); V_j is the velocity
138 value of the sampled particle, in units of m s^{-1} .

139 The average diameter is calculated as the sum of the diameters of all raindrops per unit volume divided
140 by the total number of raindrops, and the formula is given by equation 4.

$$141 \quad D_l = \frac{\sum_{i=1}^{32} N(D_i) D_i}{\sum_{i=1}^{32} N(D_i)} \quad (4)$$

142 The weighted average diameter represents the average diameter of the weighted mass of all particles
143 per unit volume relative to the total mass of particles, measured in mm. The formula is expressed in
144 equation 5.

$$145 \quad D_m = \frac{\sum_{i=1}^{32} N(D_i) D_i^4}{\sum_{i=1}^{32} N(D_i) D_i^3} \quad (5)$$

146 where D_i represents the diameter of the i -th particle, and $N(D_i)$ represents the particle number density
147 of the i -th particle diameter.

148 Precipitation intensity refers to precipitation per unit time (per hour), measured in mm h^{-1} . The
149 formula is given by equation 6.

$$150 \quad I = \frac{6\pi}{10^4} \sum_{i=1}^{32} D_i^3 V(D_i) N(D_i) \quad (6)$$

151 The radar reflectivity factor is the sum of the backscattering area of all particles per unit volume,

152 measured in $\text{mm}^{-6} \text{m}^{-3}$. The formula is expressed in equation 7.

$$Z = \sum_{i=1}^{32} N(D_i) D_i^6 \quad (7)$$

153

154 The observed raindrop spectrum is discrete, and the double parameter index, namely Exponential
155 distribution, can be used to simulate the raindrop particle size distribution. The formula is given by
156 equation 8.

$$N(D) = N_0 \times \exp(-\lambda D) \quad (8)$$

157

158 where N_0 is a number density parameter, measured in $\text{mm}^{-1} \text{m}^{-3}$. λ is a size parameter, measured in
159 mm^{-1} .

160 However, this distribution pattern has some errors compared with actual observation data when
161 describing small and large raindrops. Therefore, Ulbrich and Atlas proposed a modified raindrop
162 particle size distribution pattern. They treated the raindrop spectrum distribution as a Gamma
163 distribution to correct the distribution pattern between small and large raindrops.

164 In this case, the raindrop particle size distribution follows the Gamma distribution with three
165 parameters (Carlton and David, 1984). The formula is given by equation 9.

$$N(D) = N_0 \times D^\mu \times \exp(-\lambda D) \quad (9)$$

166

167 where μ is a dimensionless parameter referred to as the shape factor. When μ is greater than 0, the
168 curve exhibits an upward curvature; when μ is less than 0, the curve displays a downward curvature.
169 When $\mu=0$, it corresponds to an Exponential distribution.

170 Zhang (Zhang et al., 2003) pointed out a binomial relationship between μ and λ when studying the μ - λ
171 relationship of precipitation in Florida:

$$\lambda = a\mu^2 + b\mu + c \quad (10)$$

172

173 Ulbrich (Ulbrich, 1983) pointed out in his study that the μ - λ relation under Gamma distribution can be
174 expressed as:

$$D_m = \frac{4+\mu}{\lambda} \quad (11)$$

175

176 Equation (11) shows that there is a relationship between the ratio of μ and λ and the weighted average
177 diameter of mass. The Gamma distribution fit is typically applied to the observed raindrops distribution
178 $N(D)$ using the least squares or order moments method. In this study, the least square method is

179 employed to fit the Exponential and Gamma distributions.

180 **3. Result and discussion**

181 The average altitude of the Qinghai–Tibet Plateau is over 4000 m, and the terrain is complex and
 182 changeable, resulting in varying microphysical characteristics of the raindrop spectrum. Therefore,
 183 considering the unique conditions of the Qinghai–Tibet Plateau, the rain intensity calculated based on
 184 the raindrop spectrum was categorized into five grades for calculation and analysis, as presented in
 185 Table 2. The samples from the four stations in the range of 0.5–5 mm·h⁻¹ were the largest, and the
 186 obtained standard deviation values were all very small. This indicates a high consistency in rain
 187 intensity distribution under weak rain intensity. In the interval of precipitation intensity greater than 20
 188 mm h⁻¹, only two stations have samples, and one of the stations exhibits a large standard deviation.
 189 This reflects a significant inversion error in raindrop spectrum for Nyalam during short–duration heavy
 190 precipitation.

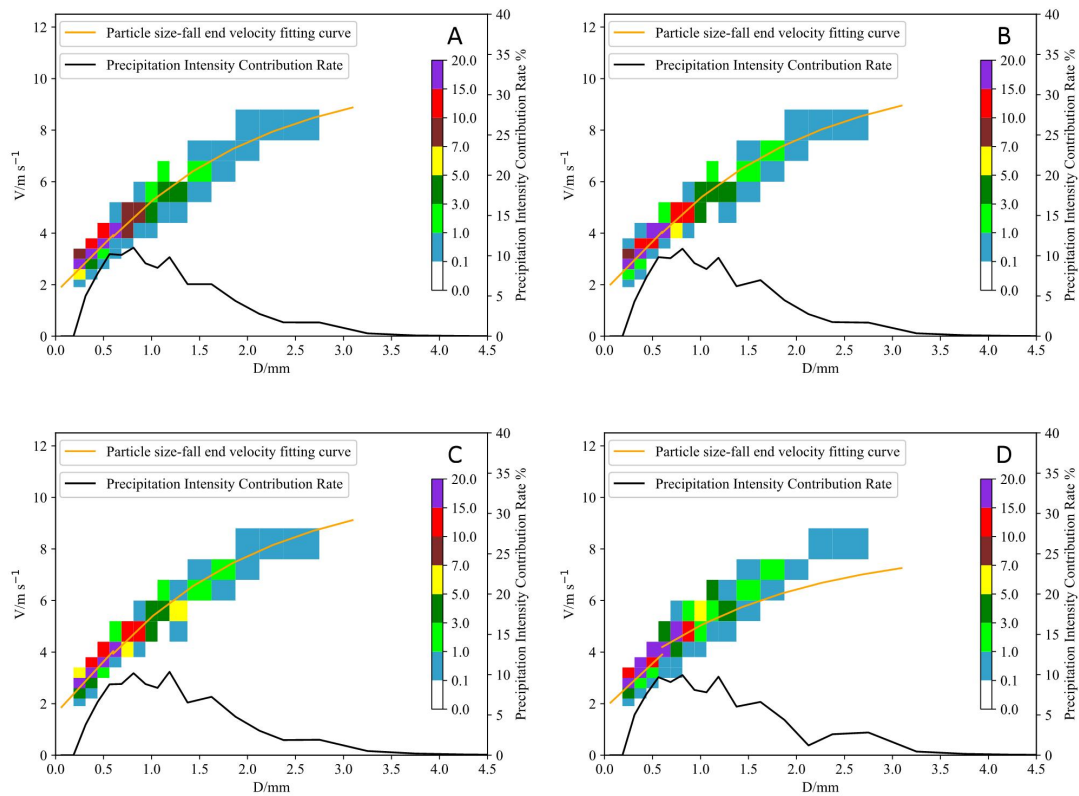
191 **Table 2: Descriptive statistics of rainfall intensity at the four stations.**

	Range (mm·h ⁻¹)	Sample Size	Mean (mm·h ⁻¹)	Standard Deviation	Precipitation (mm)
Nyalam	0.5–5	4047	2.16	1.21	146
	5–10	1358	7.38	1.28	166.6
	10–15	900	12.14	1.32	182.1
	15–20	656	17.69	1.37	193.4
	>20	960	30.63	7.99	490
Lhasa	0.5–5	3245	1.8	0.94	97.4
	5–10	180	5.87	0.77	17.6
	10–15	50	12.1	0	12.1
	15–20	0	0	0	0
	>20	0	0	0	0
Shigatse	0.5–5	7094	1.78	1.06	210.7
	5–10	584	6.37	1.11	62.02
	10–15	60	10.01	0	10.01

	15–20	0	0	0	0
	>20	0	0	0	0
	0.5–5	2389	3.27	1.5	130.1
	5–10	675	7.76	1.1	87.3
Naqu	10–15	479	13.73	1.21	109.6
	15–20	372	19.65	1.4	121.8
	>20	120	21.6	1.5	43.2

192 **3.1. Precipitation particle size, speed and rainfall intensity contribution rate distribution**

193 Figure 2 represent the mean precipitation values across the four stations. The canvas is divided into
194 several rectangular areas defined by the coordinates of the horizontal and left axes, and the color code
195 is applied to them. Each rectangular area represents a specific particle diameter and velocity. Figure 2
196 reveals that the fitting curves of particle diameter distribution and terminal velocity at the four stations
197 are approximately identical, and the terminal velocity increases with the particle diameter. Regarding
198 particle number density, it is concentrated in the area with particle size less than 1 mm, and it decreases
199 with the increase of diameter. Concerning the contribution rate of precipitation intensity, the four
200 stations exhibit a multi-peak distribution, with peak diameters at 0.812 mm and 1.375 mm. In
201 comparison with the precipitation process of convective clouds at low-altitude stations, the particle
202 size spectrum width at the four stations on the Tibetan Plateau in this analysis was notably reduced, and
203 the particle number density at the four stations with particle sizes greater than 3 mm was very low.



204
 205 **Figure 2: The average spectrum of precipitation particle size, velocity, and contribution rate distribution of**
 206 **precipitation intensity. The color bar represents the number density in units per m³. (A. Nyalam, B. Lhasa,**
 207 **C. Shigatse, and D. Naqu).**

208 Figure 3 displays the fitting relationship between the particle size of the raindrop spectrum and the
 209 falling speed at the four stations in Tibet. For particle sizes less than 1.5 mm, the particle size at the
 210 four stations essentially aligns with the final falling speed. For particle sizes greater than 1.5 mm, the
 211 speed is largest for Nyalam, followed by Naqu, and Lhasa has the smallest speed. However, under the
 212 same size, the final velocities of particles at the four stations are greater than those in Guizhou,
 213 exceeding 2 m/s. This may be attributed to the higher altitude of the four stations, which are over 3000
 214 m above sea level. This indicates that the high altitude of Tibet, due to thin air and low air pressure,
 215 results in decreased fall speed of larger particles of the same size. However, particles at lower altitudes
 216 (Shigatse and Lhasa) exhibited slightly Lower speeds than those at higher altitudes (Nyalam and Naqu).
 217 The fitting formulas for the v - D relationships at the four sites (Nyalam, Lhasa, Shigatse, and Naqu) are
 218 given by Equations 12, 13, 14, and 15, respectively. Considering the effect of air density on the fall
 219 velocity of raindrops as per Atlas et al. (1973), the correction factor $(\rho_0/\rho)^{0.4}$ is multiplied to Equations
 220 12, 13, 14, and 15, resulting in the fitting relationship curves between the particle size of the raindrop
 221 spectrum and the falling speed at the four stations in Tibet shown in Figure 3. The correction factor for

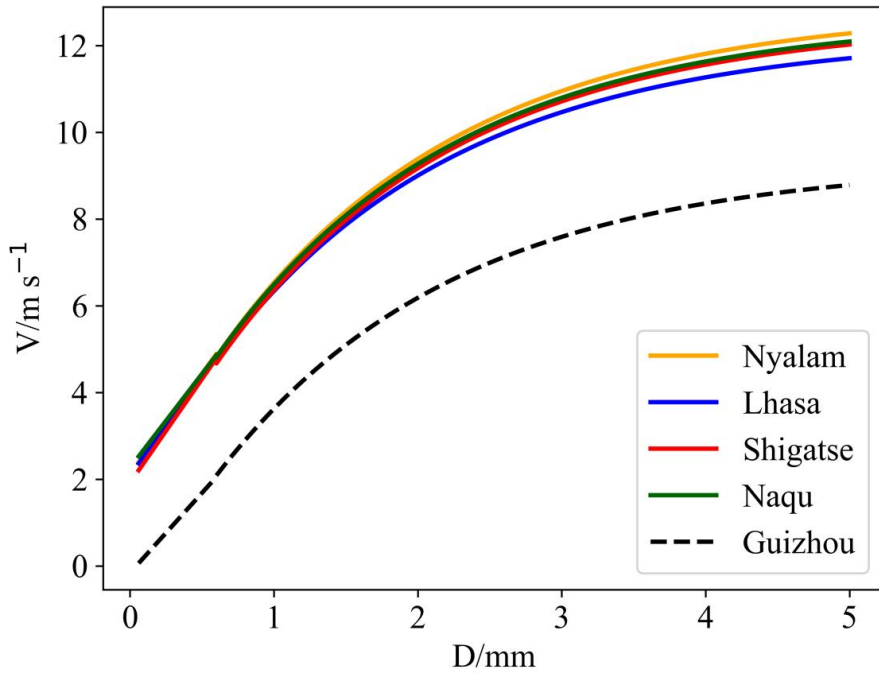
222 fall velocity considering air density is shown in Table 3.

$$223 \quad \begin{cases} v=0, & x < 0.03 \\ v = 3.720 \times (x+0.456), & 0.03 \leq x \leq 0.6 \\ v = 10.325 - 9.252 \times e^{-0.6x}, & x > 0.6 \end{cases} \quad (12)$$

$$224 \quad \begin{cases} v=0, & x < 0.03 \\ v = 3.796 \times (x+0.468), & 0.03 \leq x \leq 0.6 \\ v = 10.375 - 9.118 \times e^{-0.6x}, & x > 0.6 \end{cases} \quad (13)$$

$$225 \quad \begin{cases} v=0, & x < 0.03 \\ v = 4.035 \times (x+0.401), & 0.03 \leq x \leq 0.6 \\ v = 10.614 - 9.568 \times e^{-0.6x}, & x > 0.6 \end{cases} \quad (14)$$

$$226 \quad \begin{cases} v=0, & x < 0.03 \\ v = 3.474 \times (x+0.524), & 0.03 \leq x \leq 0.6 \\ v = 10.162 - 9.018 \times e^{-0.6x}, & x > 0.6 \end{cases} \quad (15)$$



227
228 **Figure 3: The relationship between particle size and speed at four stations.**

229 **Table 5: The correction factor for fall velocity considering air density**

Correction factor $((\rho_0/\rho)^{0.4})$			
Nyalam	Lhasa	Shigatse	Naqu
1.240	1.179	1.185	1.240

230

231 The proportion of particle number density in raindrop spectrum and the contribution rate of
 232 precipitation are shown in Table 4 and Table 5, respectively.

233 **Table 4: Percentage of particle number density.**

	Particle diameter (mm)		
	0–1 mm	1–2 mm	2–3 mm
Nyalam	93.60	6.15	0.25
Lhasa	92.41	7.24	0.35
Shigatse	91.45	8.06	0.49
Naqu	91.89	7.52	0.59

234 **Table 5: Percentage of precipitation contribution rate.**

	Particle diameter (mm)		
	0–1 mm	1–2 mm	2–3 mm
Nyalam	55.63	37.32	7.05
Lhasa	54.60	38.16	7.24
Shigatse	51.12	40.49	8.39
Naqu	54.06	37.81	8.13

235 It can be observed from Table 3 that the number of precipitation particles with a distribution of 0–1 mm
 236 constitutes the largest proportion, exceeding 91%, while the proportion of particles with a distribution
 237 of more than 3 mm is comparatively smaller, being less than 0.6%. The proportion of precipitation
 238 intensity below 1 mm constitutes over 51%, with other particles comprising less than 49%. The results
 239 indicate that the contribution of precipitation intensity on the Tibetan Plateau is primarily concentrated
 240 in small particles with a diameter less than 1 mm.

241 In contrast to the convective cloud precipitation in Zheng’an, Guizhou analyzed by Wang(Wang et al.,
 242 2020), where convective cloud particles less than 1 mm account for 64.4%, the contribution rate to
 243 precipitation is only 17%; Additionally, it significantly differs from the rainstorm in Hainan analyzed
 244 by Mao(Mao et al., 2020). Despite the proportion of less than 1mm being 82.7%, the contribution rate
 245 is only 18.2%, and the rainstorm particle size spectrum in Hainan is remarkably wide. It is evident that
 246 the precipitation characteristics of convective clouds on the Qinghai–Tibet Plateau exhibit a
 247 particularity, wherein the diameter of precipitation particles is generally small, and the precipitation of

248 small-diameter particles constitutes a substantial proportion of the total precipitation.

249 **3.2. Microphysical characteristic parameters of precipitation**

250 The calculation of microphysical parameters based on raindrop spectra is divided into five levels
251 according to different rainfall intensities. The mean diameter (D_m), average volume diameter (D_v),
252 mode diameter (D_d), dominant diameter (D_p), and median diameter (D_{nd}) were calculated for four
253 stations. Comprehensive analysis based on the characteristic parameters in Tables 6, 7, 8, and 9 shows
254 that, under the same rainfall intensity level, D_m decreases with increasing altitude. The D_m at the
255 higher-altitude Naqu and Nyalam stations is smaller than at the lower-altitude Lhasa and Shigatse
256 stations. Under the same rainfall intensity level, D_v increases with altitude, with the smallest value at
257 the low-altitude Lhasa station and the largest at the high-altitude Naqu station. When the rainfall
258 intensity is less than $\text{mm}\cdot\text{h}^{-1}$, D_d increases with altitude (except for the Nyalam station), with the
259 largest value at the Naqu station and the smallest at the Lhasa station, with the Shigatse station in
260 between. When the rainfall intensity is greater than $10\text{mm}\cdot\text{h}^{-1}$, D_d decreases with altitude, with the
261 largest value at the Lhasa station and the smallest at the Nyalam station, with the Shigatse and Naqu
262 stations in between. When the rainfall intensity is less than $10\text{ mm}\cdot\text{h}^{-1}$, D_p does not show a significant
263 difference with altitude under the same rainfall intensity level. However, when the rainfall intensity is
264 greater than $10\text{ mm}\cdot\text{h}^{-1}$, D_p increases with altitude under the same rainfall intensity level (except for
265 the Nyalam station). For the lower-altitude Lhasa and Shigatse stations, there is no significant
266 difference in parameters under the same rainfall intensity. In contrast, for the higher-altitude Naqu and
267 Nyalam stations, there are relatively obvious differences in parameters under the same rainfall intensity,
268 with the Nyalam station's values being significantly smaller than those of the Naqu station. The reason
269 for the smaller values at the Nyalam station compared to the nearby altitude Naqu station might be due
270 to its unique geographical conditions. The above analysis indicates a strong correlation between
271 altitude and these microphysical parameters. D_m shows a negative correlation with altitude under the
272 same rainfall intensity, while D_v shows a positive correlation with altitude. For D_d and D_p , using 10
273 $\text{mm}\cdot\text{h}^{-1}$ as the dividing line, there are different correlations with altitude under the same rainfall
274 intensity level. Additionally, when the altitude is below 4000 m, there is no significant difference in
275 characteristic diameters under the same rainfall intensity. Conversely, when the altitude is above 4000
276 m, the differences in characteristic diameters become more pronounced.

277 **Table 6: Microphysical parameters of the Lhasa station.**

	Range	Dm	Dv	Dd	Dp	Dnd
	(mm·h ⁻¹)					
Lhasa	0.5-5	0.636	1.744	0.470	1.277	1.105
	5-10	0.809	2.058	0.671	1.869	1.628
	10-15	0.981	2.231	1.096	2.229	2.058
	15-20	1.008	2.288	1.069	2.256	2.095
	>20	1.063	2.421	1.331	2.744	2.580

278 **Table 7: Microphysical parameters of the Shigatse station.**

	Range	Dm	Dv	Dd	Dp	Dnd
	(mm·h ⁻¹)					
Shigatse	0.5-5	0.641	1.748	0.473	1.291	1.126
	5-10	0.815	2.044	0.685	1.901	1.639
	10-15	0.970	2.216	1.041	2.293	2.088
	15-20	1.000	2.298	1.277	2.612	2.292
	>20	1.045	2.409	1.200	2.833	2.566

279 **Table 8: Microphysical parameters of the Nyalam station.**

	Range	Dm	Dv	Dd	Dp	Dnd
	(mm·h ⁻¹)					
Nyalam	0.5-5	0.593	1.764	0.415	1.282	1.088
	5-10	0.725	2.064	0.498	1.865	1.574
	10-15	0.823	2.163	0.601	2.062	1.720
	15-20	0.905	2.217	0.846	2.351	2.022
	>20	0	0	0	0	0

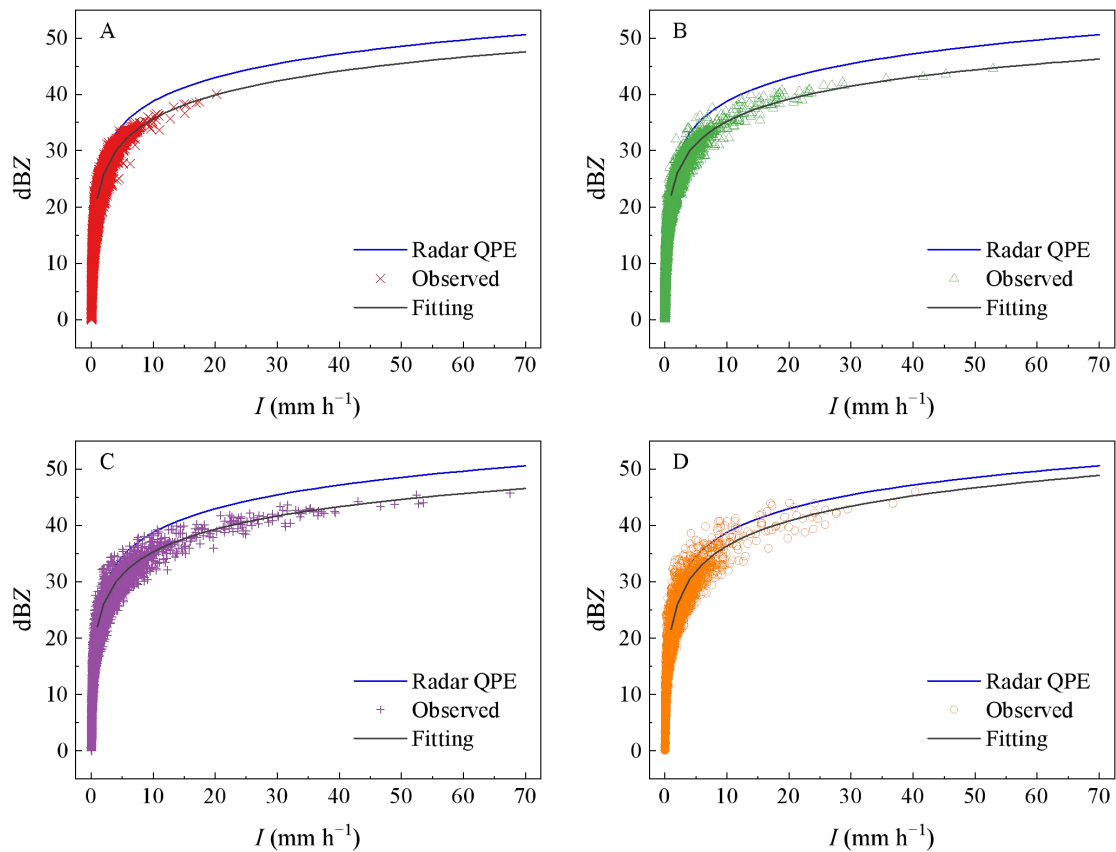
280 **Table 9: Microphysical parameters of the Naqu station.**

	Range	Dm	Dv	Dd	Dp	Dnd
	(mm·h ⁻¹)					
Naqu	0.5-5	0.621	1.758	0.491	1.268	1.110
	5-10	0.808	2.071	0.777	1.730	2.022

	10-15	0.922	2.250	0.947	2.434	2.205
	15-20	0.970	2.313	1.005	2.595	2.291
	>20	1.043	2.479	1.166	3.004	2.673

281 **3.3. Z-I relation distribution**

282 Utilizing Formulae (6) and (7), the radar reflectivity (Z) and precipitation intensity (I) are calculated
 283 independently, and the data undergo fitting. The results are depicted in Figure 4.



284
 285 **Figure 4: The Z-I relationships at four stations. (A. Nyalam, B. Lhasa, C. Shigatse, and D. Naqu)**

286 Figure 4 reveals that the suggested reference relation $Z=300 \times I^{1.4}$ inaccurately predicts precipitation,
 287 leading to an underestimation of precipitation intensity under identical radar reflectivity. With identical
 288 radar reflectance, the precipitation intensity is highest in Lhasa, followed by Shigatse, while the
 289 smallest precipitation intensity was observed in Naqu.

290 Table 7 shows the results of fitted Z-I relationships. Analyzing the altitude based differences in the Z-I
 291 relationship, the a and b coefficients are similar for the station at 3653 m (Lhasa) and the station at
 292 3910 m (Shigatse), while a and b for the station at 4519 m (Nyalam) and the station at 4560 m (Naqu)
 293 are close. This observation indicates that the fitting parameter a is notably smaller, and the fitting

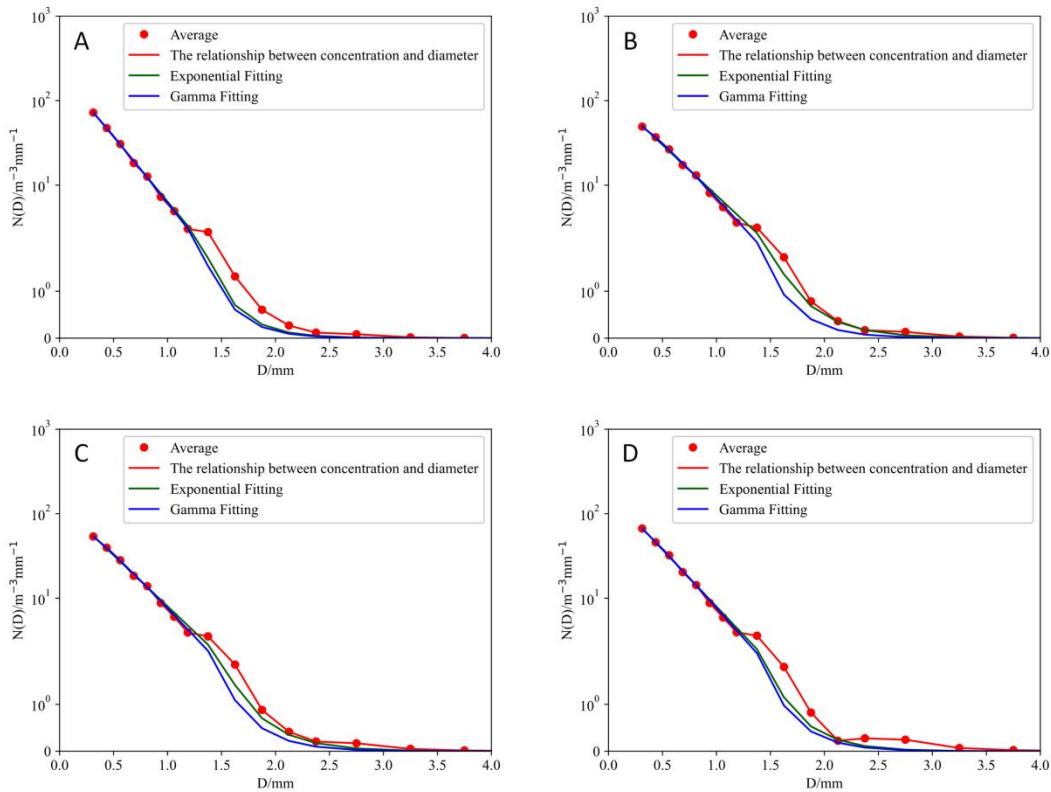
294 parameter b is larger for stations at higher altitudes.

295 **Table 10: Z-I relationship fitting results.**

		$Z = aI^b$	
		Fitting	
		a	b
Nyalam	$Z=143.01 \times I^{1.41}$	143.01	1.41
Lhasa	$Z=162.56 \times I^{1.31}$	162.56	1.31
Shigatse	$Z=160.21 \times I^{1.33}$	160.21	1.33
Naqu	$Z=143.81 \times I^{1.48}$	143.81	1.48

296 **3.4. Precipitation particle distribution fitting**

297 According to Formulas (8) and (9), the least squares method is applied to fit the Exponential and
 298 Gamma distributions of the mean raindrop spectrum of precipitation at the four stations. The results are
 299 presented in Figure 5 and Table 7.



300 **Figure 5: Exponential and Gamma intriptions for precipitation (A. Nyalam, B. Lhasa, C. Shigatse, and D.**
 301 **Naqu).**

303 As indicated in Table 8, μ decreases with increasing altitude in the Gamma distribution. A smaller μ
 304 corresponds to a wider raindrop spectrum, signifying that the diameter of raindrops increases with
 305 altitude. The raindrop diameter at higher altitudes is larger, corresponding to the precipitation

306 microphysical characteristics calculated in Table 6. Conversely, the fitting results of the Exponential
307 distribution show that N_0 and λ exhibit a clear increasing trend with height. In Figure 5, the abscissa
308 represents particle diameter, and the ordinate represents particle number density. The curve trends at the
309 four stations are relatively consistent. For Nyalam station, the Exponential distribution is given by
310 $N(D)=218.78 \times e^{-3.53D}$, and the Gamma distribution is $N(D)=282.14 \times D^{0.15} \times e^{-3.82D}$. For Lhasa
311 station, the Exponential distribution is $N(D)=118.70 \times e^{-2.75D}$, and the Gamma distribution is
312 $N(D)=250.40 \times D^{0.43} \times e^{-3.56D}$. For Shigatse station, the Exponential distribution is
313 $N(D)=130.35 \times e^{-2.79D}$, and the Gamma distribution is $N(D)=216.08 \times D^{0.29} \times e^{-3.35D}$. Finally, for
314 Naqu station, the Exponential distribution is $N(D)=177.22 \times e^{-3.10D}$, and the Gamma distribution is
315 $N(D)=238.95 \times D^{0.17} \times e^{-3.44D}$. In the Gamma distribution, two parameters, μ and λ , represent the
316 curve shape factor and particle scale parameters, respectively, as shown in Equation (9). According to
317 Equation (10), the two parameters μ and λ for the four stations are fitted with an analytical binomial
318 relationship, and the coefficients are presented in Table 9.

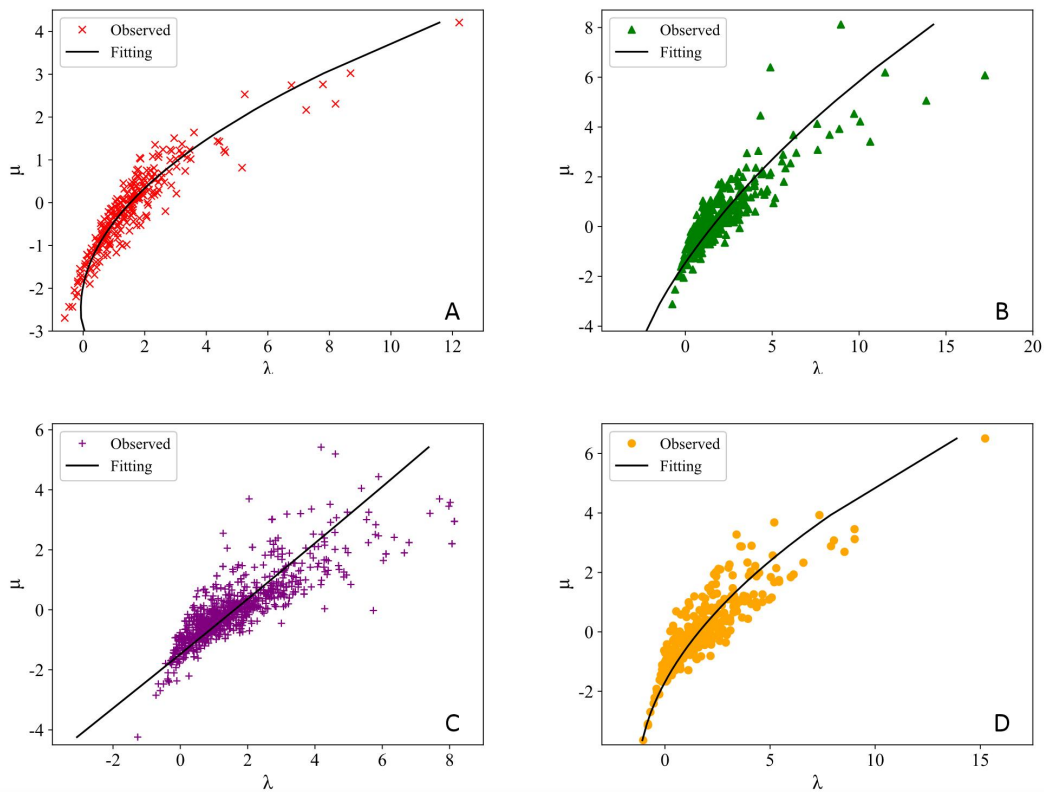
319 **Table 11: Gamma fitting and Exponential fitting results.**

	Gamma			Exponential	
	N_0	μ	λ	N_0	λ
Nyalam	284.90	0.15	3.83	218.93	3.53
Lhasa	253.26	0.44	3.59	118.81	2.75
Shigatse	217.69	0.30	3.35	130.45	2.79
Naqu	240.91	0.18	3.45	177.34	3.10

320 **Table 12: μ and λ binomial parameters**

	$\lambda = a\mu^2 + b\mu + c$		
	a	b	c
Nyalam	0.2816	1.2798	1.5074
Lhasa	0.1717	1.0589	1.3983
Shigatse	0.0221	1.1215	1.6002
Naqu	0.0155	1.2141	1.7599

321 It can be observed from Figure 6 that, although the four curves bend towards the lambda axis, the
322 degree of bending varies. The curves for Shigatse exhibit nearly straight curves, whereas the curves for
323 Nyalam and Naqu are more pronounced in their curvature towards the lambda axis. The μ - λ
324 relationship varies among the four stations, and this variation is associated with the mass-weighted
325 diameter. Eq. (11) indicates that when λ remains constant, a higher μ value corresponds to a greater
326 mass-weighted average diameter.



327
328

Figure 6: μ - λ relationship (A. Nyalam, B. Lhasa, C. Shigatse, D. Naqu).

329 4. Conclusions

330 In this study, we conducted a statistical analysis of raindrop spectrum data above light and moderate
 331 rain at four sites in Tibet, considering different heights, latitudes, and longitudes. The analysis includes
 332 precipitation particle size distribution, particle landing speed, precipitation particle number density, and
 333 rainfall intensity at the end. Additionally, the relationship between Z-I distribution and rainfall rate,
 334 precipitation particle distribution fitting, and analysis of Gamma distribution μ - λ parameters for the
 335 precipitation raindrop spectrum characteristics at the four stations are examined. A comparison is made
 336 between the data from the four stations on the Qinghai-Tibet Plateau and some non-plateau areas.
 337 Simultaneously, the analysis of raindrop spectrum data at the Naqu station reveals certain similarities
 338 with previous studies (indicating convective cloud as the primary precipitation at Naqu station).
 339 However, some differences are noted, such as the mean spectral width of convective precipitation at the
 340 Naqu station being relatively narrow.

341 The relationship between precipitation particle size and particle landing velocity at the four stations
 342 indicates that the terminal velocity of the four stations essentially coincided when the particle size was

343 less than 1.5 mm. For particle sizes greater than 1.5 mm, the terminal velocity of particles at the four
344 stations is faster at high altitudes than at medium and low altitudes. At the four stations, the proportion
345 of precipitation raindrop spectral particle size less than 1 mm exceeded 91%, and the contribution rate
346 of precipitation was more than 51%. The characteristics of convective cloud precipitation over the
347 Tibetan Plateau exhibit peculiarities that differ from the raindrop spectrum characteristics in the
348 low-altitude areas of the mainland.

349 The six microphysical characteristics at the four stations have different correlation relationships with
350 altitude under different rainfall intensities. D_m exhibits a negative correlation with altitude at the same
351 rainfall intensity; in contrast, D_v shows a positive correlation with altitude. For microphysical
352 parameters such as D_d and D_p , a rainfall intensity of $10 \text{ mm}\cdot\text{h}^{-1}$ serves as the boundary line, and they
353 have different correlation relationships with altitude under the same rainfall intensity level. Regarding
354 the fitted $Z-I$ relationship, the fitting parameter a at the high-altitude station is significantly smaller,
355 while the fitting parameter b is larger. The particle spectrum of high-altitude stations is broader, with a
356 larger equivalent diameter, and the reflectivity of high-altitude stations is significantly higher than that
357 of low-altitude stations.

358 The concentration of small raindrops (less than 1 mm) in the raindrop spectrum of high-altitude
359 stations on the Tibetan Plateau was higher. Both the Exponential distribution and the Gamma
360 distribution exhibit good fitting effects for low-altitude stations. Overall, the Exponential fit performed
361 better. In the relationship between the μ and λ of the two parameters in the Gamma distribution, the
362 larger the μ , the larger the weighted average diameter of the mass when the λ remains constant. In other
363 words, the greater the μ , the greater the precipitation intensity when λ remains unchanged.

364 **Data Availability Statement**

365 The data used to support the findings of this study are available from the corresponding author upon
366 request.

367 **Author Contributions**

368 Conceptualization, F.W. and G.C.; methodology, F.W. and Q.W.; software, Y.H., Y.D and Q.W.;
369 writing—review and editing, F.W., Y.H., Y.D and Y.C.; resources, T.Z. and J.L.; supervision, T.Z. and

370 G.C. All authors have read and agreed to the published version of the manuscript.

371 **Competing interests**

372 The contact author has declared that none of the authors has any competing interests.

373 **Disclaimer**

374 Publisher's note: Copernicus Publications remains neutral with regard to jurisdictional claims made in
375 the text, published maps, institutional affiliations, or any other geographical representation in this paper.

376 While Copernicus Publications makes every effort to include appropriate place names, the final
377 responsibility lies with the authors.

378 **Acknowledgements**

379 We thank the Tibet Meteorological Bureau for the raindrop spectrum data, and the students and
380 teachers of Chengdu University of Information Technology for their help.

381 **Financial support**

382 This research was funded by the Open Fund project for Key Laboratory of Land Surface Process and
383 Climate Change in Cold and Arid Regions, Chinese Academy of Sciences (LPCC2020009), and the
384 Natural Science Foundation of Sichuan Province (2022NSFSC0208) and National Natural Science
385 Foundation of China (42075001).

386 **References**

387 Atlas, D., Srivastava, R. C., and Sekhon, R. S.: Doppler characteristics of precipitation at vertical
388 incidence, *Rev. Geophys.*, 1973, 11, 1-35, doi:10.1029/RG011i001p00001, 1973.

389 Battaglia, A., Rustemeier, E., Tokay, A., Blahak, U., and Simmer, C: PARSIVEL snow observations: A
390 critical assessment, *J. Atmos. Ocean. Tech.*, 27, 333-344, doi: 10.1175/2009JTECHA1332.1, 2010.

391 Chang, Y., and Guo, X. L.: Characteristics of convective cloud and precipitation during summer time at
392 Nagqu over Tibetan Plateau, *Sci. Bull.*, 61, 1706–1720, doi:10.1360/N972015-01292, 2016.

393 Carlton, W. U., and David, A.: Assessment of the contribution of differential polarization to improved

394 rainfall measurements, *Radio Science*, 19, 49-57, doi:10.1029/RS019i001p00049, 1984.

395 Jiang, J. X., and Fan, M. Z.: Convective clouds and mesoscale convective systems over the Tibetan
396 Plateau in summer, *Chin. J. Atmos. Sci*, 26, 263-270, doi:10.3878/j.issn.1006-9895.2002.02.12, 2002.

397 Kruger, A., and Krajewski, W. F.: Two-Dimensional Video Disdrometer: A Description, *J. Atmos.*
398 *Ocean. Tech*, 19, 602-617, doi:10.1175/1520-0426(2002)019<0602:TDVDAD>2.0.CO, 2002.

399 Li, D., Bai, A. J., Xue, Y. J., and Wang, P.: Comparative analysis on characteristics of summer
400 convective precipitation over Ti-betan Plateau and Sichuan Basin, *Meteor. Mon.*, 40, 280-289, doi:
401 10.7519/j.issn.1000-0526.2014.03.003, 2014.

402 Li, L. G., and De, L. G. E.: Analyses of microphysical features for spring precipitation cloud layers in
403 east of Qinghai, *Plateau Meteorology*, 20, 191-196, doi:10.3321/j.issn:1000-0534.2001.02.013, 2001.

404 Liu, L. P., Zheng, J. F., Ruan, Z., Cui, Z. H., Hu, Z. Q., Wu, S. H., et al.: The preliminary analyses of
405 the cloud properties over the Tibetan Plateau from the field experiments in clouds precipitation with the
406 various radars, *Acta. Meteor. Sin*, 73, 635-647, doi:10.11676/qxxb2015.041, 2015.

407 Li, S. S., Wang, X. F., Wan, R., and Li, G. P.: The Characteristics of Raindrop Spectrum in Different
408 Altitude Region on the Eastern Slope of Qinghai-Xizang Plateau, *Plateau Meteorology*, 39, 899-911,
409 doi:10.7522/j.issn.1000-0534.2019.00086, 2020.

410 Marshall, J. S., and Palmer, W. M.: The Distribution of Raindrops with Size, *J. Meteor*, 5, 165-166,
411 doi: 10.1175/1520-0469(1948)005<0165:TDORWS>2.0.CO;1948

412 Mao, Z. Y., Huang, G. R., Huang, Y. B., Li, G. W., and Xing, F. H.: Characteristics Analysis of
413 Raindrop Size Distribution during Hainan Autumn-Rainstorm Process, *Natural Science Journal of*
414 *Hainan University*, 38, 59-66, doi:10.15886/j.cnki.hdxzbkb.2020.0009, 2020.

415 Ruan, Z., Jin, L., Ge, R. S., Li, F., and Wu, J.: The C-band FMCW pointing weather radar system and
416 its observation experiment, *Acta. Meteor. Sin*, 3, 577-592, doi:10.11676/qxxb2015.039, 2015.

417 Shu, L., Li, M. S., Hua, S., Suo, L. J. C., Lv, Z., Fu, W., et al.: Statistical Characteristics of Raindrop
418 Size Distribution and Microphysical Structure of Cloud in Yushu Region of Qinghai Tibet Plateau,
419 *Advances in Meteorological Science and Technology*, 11, 113-121+134,
420 doi:10.3969/j.issn.2095-1973.2021.04.016, 2021.

421 Shi, J. S., Zhang, W., Chen, T. Y., Bi, J. R., and He, M.: Raindrop-size distribution characteristics of the
422 northern face of Qilian Mountains in the summer of 2006, *J. Lanzhou University(Natural Sciences)*, 44,
423 55-61, doi: 10.3321/j.issn:0455-2059.2008.04.011, 2008.

424 Ulbrich, C. W.: Natural Variations in the Analytical Form of the Raindrop Size Distribution, *J. Climate*.
425 *Appl. Meteor*, 22, 1764-1775, doi:10.1175/1520-0450(1983)022<1764:NVITAF>2.0.CO;2, 1983.

426 Wang, F. Z., Wang, Q. S., He, S., Gu, X. P., and Yu, F.: Analysis of Summer Raindrop Spectrum
427 Characteristics of Zheng'an in Guizhou, *J. Chengdu University. Inf Technology*, 35, 689-696,
428 doi:10.16836/j.cnki.jcuit.2020.06.016, 2020.

429 Xu, X. D., and Chen, L. S.: Advances of study on Tibetan Plateau experiment of atmospheric sciences,
430 *J. Appl. Meteor. Sci*, 17, 756-772, doi:10.3969/j.issn.1001-7313.2006.06.013, 2006

431 Xiong, J. N., Li, W., Liu, Z. Q., Cheng, W. M., Fan, C. K., and Zhang, H.: Monitoring and analysis of
432 historical drought in southeast Tibet based on multi--source data, *Arid Land Geography*, 42, 735-744,
433 doi:10.12118/j.issn.1000-6060.2019.04.04, 2019.

434 Yu, J. Y., Li, M. S., and Yin, S. C.: Analysis of Cloud Precipitation Microscopic Characteristic
435 Raindrop Spectrum in Nagqu Area of Qinghai-Tibet Plateau, *J. Chengdu University. Inf Technology*, 35,
436 188-194, doi:10.16836/j.cnki.jcuit.2020.02.010, 2020.

437 Zhang, N. J., Xiao, T. G., and Jia, L.: Spatial and Temporal Characteristics of Precipitation in the Tibet
438 Plateau from 1979 to 2016, *J. Arid. Meteorology*, 36, 373-382,
439 doi:10.11755/j.issn.1006-7639(2018)-03-0373, 2018.

440 Zhang, G., Vivekanandan, J., Brandes, E. A., Meneghini, R., and Kozu, T.: The Shape-Slope Relation
441 in Observed Gamma Raindrop Size Distributions: Statistical Error or Useful Information?, *J. Atmos.*
442 *Ocean. Tech*, 20, 1106-1119, doi:10.1175/1520-0426(2003)020<1106:TSRIOG>2.0.CO;2, 2003.